Pergamon

Int. J. Heat Mass Transfer. Vol. 40, No. 17, pp. 4239–4249, 1997

Printed in Great Britain
0017–9310/97 $17.00+0.00

PII: S0017–9310(97)00072–0

Natural convection of micropolar fluids in an enclosure with heat sources

TSAN-HUI HSU and PAO-TUNG HSU

Department of Mechanical Engineering, National Kaohsiung Institute of Technology, Kaohsiung, Taiwan, Republic of China

and

SO-YENN TSAI

Department of Tool and Die-making Engineering, National Kaohsiung Institute of Technology, Kaohsiung, Taiwan, Republic of China

(*Received* 16 *March* 1995)

Abstract—Numerical study of natural convection flow in a tilting enclosure filled with micropolar fluids has been investigated. The enclosure is equipped with a single or multiple uniform heat sources. A two-dimensional, steady and laminar flow model is simulated. The heat transfer characteristic and flow phenomenon are presented for range values of the controlled parameters and situations, such as *Ra* number, tilting angle of the enclosure and various material parameters of the fluid. The results indicate that dependence of microrotation term and heat transfer on microstructure parameters is significant. The effects of heat source locations and arrangement of multiple heat sources are studied to arrive at qualitative suggestions that may improve the cooling design of the system. The effect of the microrotation boundary conditions on heat transfer is discussed as well. © 1997 Elsevier Science Ltd.

INTRODUCTION

The natural convection in enclosures has become increasingly important in engineering applications in recent years [1, 2]. In particular, as high power electronic packaging and component density continue to increase substantially with the fast growth of electronic technology, effective cooling of electronic equipment has become warranted. The application of natural convection cooling for electronic equipment ranges from individual transistors to mainframe computers and from energy supplies to telephone switch boards.

The study of Chu *et al.* [3] represented a major contribution to the natural convection in rectangular enclosures with concentrated heat sources. The numerical solutions, which were in agreement with the experimental work, presented the effect of heat size, location, aspect ratio and the endwall thermal boundary conditions on the flow structure and heat transfer in rectangular channels. Turner and Flack [4] experimentally confirmed the results observed by Chu *et al.*, but for higher Grashof numbers ($5 \times 10^6 \leqq Gr \leqq 10^9$). Afrid and Zebib [5] discussed a numerical study of natural convection air cooling of a single and multiple uniformly heat sources in an open region. They found that the layout, thickness and strength of the heat sources have significant effect on the flow structure and source surface temperature. Natural convection in a vertical cavity with an array of discrete heat sources was experimentally studied by Keyhani *et al.* [6]. Refai and Yovanovich [7] presented the heat transfer from a discrete heat source in a square enclosure. Relationships between *Nu* and *Ra* based on different scale lengths were examined therein.

The theory of micropolar fluids developed by Eringen [8–10] has been a popular area of research in recent years. In this theory, the local effects arising from microstructure and intrinsic motions of the fluid elements were taken into account. It is expected to describe successfully the non-Newtonian behavior of certain fluids, such as liquid crystal, ferro liquids, colloidal fluids and liquid with polymer additives. Recently, Jena and Bhattacharyya [11] studied the influence of microstructure on the thermal convection in a rectangular box heated from below with Galerkin method and obtained critical Rayleigh numbers for various material parameters. Natural convection of micropolar fluids in a square cavity with differentially heated endwalls was investigated by Chen and Hsu [12]. It was found that the heat transfer rate of micropolar fluid is lower than that of Newtonian fluid.

The present study is concerned with the simulation of the flow and temperature fields of micropolar fluid in a tilting rectangular enclosure under various natural and artificial conditions. The effect of material parameters of micropolar fluid on the thermal characteristics is investigated for different Rayleigh numbers.

NOMENCLATURE

A	aspect ratio, H/L
B	material parameter, L^2/j
H	enclosure height
h	heat transfer coefficient
j	microinertia per unit mass
k	thermal conductivity of the fluid
K_v	vortex viscosity
L	enclosure length
n	constant, equations (12a) and (12b)
$\tilde{n}$	normal coordinate
Nu	local Nusselt number
$\overline{Nu}$	average Nusselt number
Pr	Prandtl number, ν/α
q	heat flux
Ra	Rayleigh number: $g\beta(T_h-T_c)L^3/(\alpha\nu)$ for isothermal case; $g\beta qL^4/(\alpha\nu k)$ for isoflux case
s	length of heat source
T	temperature
t	time
U	dimensionless velocity component in x-direction, Lu/α
u	velocity component in x-direction
V	dimensionless velocity component in y-direction, Lv/α
v	velocity component in y-direction
X	dimensionless Cartesian coordinate in x-direction, x/L
x	Cartesian coordinate
Y	dimensionless Cartesian coordinate in y-direction, y/L
y	Cartesian coordinate
$Y1$	dimensionless coordinate, y_1/H
$Y2$	dimensionless coordinate, y_2/H.

Greek symbols

α	thermal diffusivity of the fluid
β	coefficient of the thermal expansion
σ	angular velocity component
θ	dimensionless temperature: $(T-T_c)/(T_h-T_c)$ for isothermal case; $k(T-T_c)/(qL)$ for isoflux case
τ	dimensionless time, $\alpha t/L^2$
μ	dynamic viscosity
ν	kinematic viscosity, μ/ρ
υ	dimensionless angular velocity, $L^2\sigma/\alpha$
φ	general dependent variable, equations (15) and (16)
ϕ	general dependent variable, equations (17) and (18)
ψ	stream function
Ψ	dimensionless stream function, ψ/α
ω	vorticity, $\omega = \partial v/\partial x - \partial u/\partial y$
Ω	dimensionless vorticity, $(L^2\omega)/\alpha$
γ	spin gradient viscosity
ξ	tilting angle of enclosure
Δ	material parameter, K_v/μ
λ	material parameter, $\gamma/(j\mu)$
ε	s/H.

Subscript

1, 2	denote heat source 1 and 2 separately.

In order to show the fundamental flow field caused by discrete heat sources, several arrangements for the heat source in the system are achieved. The results for heat transfer phenomenon in the enclosure with Newtonian fluid have been presented for qualitative comparison.

ANALYSIS

The configuration and coordinate system of the problem are shown in Fig. 1. The enclosure is arranged to have a tilting angle ξ with the horizontal plane. The right vertical surface is maintained at constant temperature T_c and the left one, with discrete heat sources (isoflux q or isothermal T_h, with $T_h > T_c$), is assumed to be adiabatic. The two horizontal surfaces are kept insulated. The flow is assumed to be two-dimensional, laminar and the fluid properties are assumed to be constant. The variation of density with temperature is calculated using the Boussinesq approximation and the viscous dissipation as well as micropolar heat conduction effect are neglected. The governing equations for micropolar fluid in an enclosure can be described in dimensionless form by:

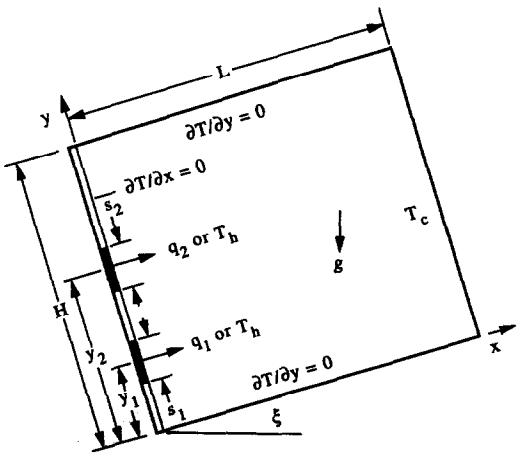

Fig. 1. Physical model.

$$\nabla^2\Psi = -\Omega \tag{1}$$

$$\frac{\partial\Omega}{\partial\tau}+U\frac{\partial\Omega}{\partial X}+V\frac{\partial\Omega}{\partial Y}=Pr(1+\Delta)\nabla^2\Omega-Pr\Delta\nabla^2\Omega + PrRa\left(\frac{\partial\theta}{\partial X}\cos\xi-\frac{\partial\theta}{\partial Y}\sin\xi\right) \tag{2}$$

$$\frac{\partial\upsilon}{\partial\tau}+U\frac{\partial\upsilon}{\partial X}+V\frac{\partial\upsilon}{\partial Y}=\Delta BPr(\Omega-2\upsilon)+Pr\lambda\nabla^2\upsilon \tag{3}$$

$$\frac{\partial\theta}{\partial\tau}+U\frac{\partial\theta}{\partial X}+V\frac{\partial\theta}{\partial Y}=\nabla^2\theta \tag{4}$$

where

$$U=\frac{\partial\Psi}{\partial Y}\quad V=-\frac{\partial\Psi}{\partial X} \tag{5}$$

and with the dimensionless variables defined as

$$X=\frac{x}{L},\quad Y=\frac{y}{L},\quad \tau=\frac{\alpha t}{L^2},\quad u=\frac{Lu}{\alpha},$$

$$V=\frac{Lv}{\alpha},\quad \Omega=\frac{L^2\omega}{\alpha},\quad \Psi=\frac{\psi}{\alpha},\quad \upsilon=\frac{L^2\sigma}{\alpha}$$

$$\theta=\frac{T-T_c}{T_h-T_c}\quad\text{(isothermal heat source) or}$$

$$\theta=\frac{k(T-T_c)}{qL}\quad\text{(isoflux heat source).} \tag{6}$$

The boundary conditions are as follows. At the horizontal surface, $Y = 0, A$:

$$U=V=\Psi=0,\quad \frac{\partial\theta}{\partial Y}=0. \tag{7}$$

At the left boundary:

$$X=0,\quad 0\leqq Y\leqq Y1-\frac{\varepsilon_1}{2},$$

$$Y1+\frac{\varepsilon_1}{2}\leqq Y\leqq Y2-\frac{\varepsilon_2}{2}\quad\text{and}\quad Y2+\frac{\varepsilon_2}{2}\leqq Y\leqq A:$$

$$U=V=\Psi=0\quad\frac{\partial\theta}{\partial X}=0. \tag{8}$$

At the right boundary, $X = 1$:

$$U=V=\Psi=\theta=0. \tag{9}$$

The condition for the heat source is

$$\theta=1\quad\text{(isothermal case)}$$

$$\text{or}\quad\frac{\partial\theta}{\partial X}=-1\quad\text{(isoflux case).} \tag{10}$$

The following boundary condition is available for vorticity, i.e.

$$\Omega=-\frac{\partial^2\Psi}{\partial\tilde{n}^2} \tag{11}$$

where $\tilde{n}$ denotes the direction perpendicular to the surface.

For the microrotation, the following boundary conditions are assumed.

$$\upsilon=n\frac{\partial V}{\partial X}\quad\text{at } X=0,1 \tag{12a}$$

$$\upsilon=-n\frac{\partial U}{\partial Y}\quad\text{at } Y=0,A \tag{12b}$$

where n is a constant and $0 \leqq n \leqq 1$. The case $n = 0$ represents concentrate particle flows in which the microelements close to the wall are unable to rotate [13]. The case corresponding to $n = 0.5$ results in the vanishing of antisymmetric part of the stress tensor and represents weak concentrations [14]. The case $n = 1$, as suggested by Peddieson [15], is applicable to the modeling of turbulent boundary layer flows.

The governing parameters in the preceding equations are Prandtl number Pr, Rayleigh number Ra and various material parameters Δ, B and λ, which are defined in the Nomenclature.

The local Nusselt number Nu for the heated wall is calculated by $Nu = hL/k$

$$=-\frac{\partial\theta}{\partial X}\bigg|_{X=0}\quad\text{for isothermal case} \tag{13a}$$

and

$$=\frac{1}{\theta}\bigg|_{X=0}\quad\text{for isoflux case.} \tag{13b}$$

Furthermore the average Nusselt number is defined as

$$\overline{Nu}=\frac{1}{S}\int_0^S Nu\,\mathrm{d}y=\frac{1}{A\varepsilon}\int_0^{A\varepsilon} Nu\,\mathrm{d}Y. \tag{14}$$

NUMERICAL PROCEDURE

The coupled equations (1)–(4) with the associated boundary conditions are solved by the cubic spline collocation method [16]. The spline alternating direction implicit procedure (SADI) is adopted to perform the numerical computation. An accuracy test of grid fineness is made for the arrangements of 21×21, 31×31 and 41×41. It is found that the results for grids of 21×21 and 41×41 reveal difference less than 1% in the isotherms and local Nu values at $Ra = 10^5$. Thus, an arrangement of 21×21 nonuniform mesh size is used in most cases for the present work. However, a finer mesh size is needed for large Rayleigh number, e.g. mesh size of 41×41 is used for $Ra = 10^7$.

The governing equations (1)–(4) are first put in the following form:

$$\varphi_{ij}^{p+1/2}=F_{ij}^p+G_{ij}^p m_{\varphi ij}^{p+1/2}+S_{ij}^p M_{\varphi ij}^{p+1/2} \tag{15}$$

$$\varphi_{ij}^{p+1}=F_{ij}^{p+1/2}+G_{ij}^{p+1/2} m_{\varphi ij}^{p+1}+S_{ij}^{p+1/2} M_{\varphi ij}^{p+1} \tag{16}$$

where i and j refer to the computational nodes, p is the time step, φ represents Ψ, Ω, υ and θ, and m and

M are the first and second derivatives of φ with respect to X and Y, respectively. F_{ij}, G_{ij} and S_{ij} are the known coefficients evaluated at previous time step. In order to put equation (1) in the previous form, (15) and (16), a fictitious time technique is employed.

After transforming by using cubic spline collocation relations described in [16], equations (15) and (16) might be rewritten in tridiagonal form as:

$$A_{j-1}\phi_{ij-1}^{p+1/2} + B_j\phi_{ij}^{p+1/2} + C_{j+1}\phi_{ij+1}^{p+1/2} = D_j \quad (17)$$

$$A_{i-1}\phi_{i-1j}^{p+1} + B_i\phi_{ij}^{p+1} + C_{i+1}\phi_{i+1j}^{p+1} = D_i \quad (18)$$

where ϕ represents the function Ψ, Ω, υ and θ or its first two derivatives. Thus, equations (17) and (18) are easily solved by using the Thomas algorithm. The solution procedures are iterated until the maximum relative change in temperature and flow fields in the enclosure satisfy the following convergence criterion, i.e.

$$\left|\frac{\phi_{ij}^{z} - \phi_{ij}^{z-1}}{\phi_{\max}^{z}}\right| \leqslant 10^{-5} \quad (19)$$

where ϕ refers to Ω, υ and θ, and z denotes the number of iteration. Since the steady solutions are the main interest in the present work, it is assumed that the solutions have been obtained when the following average criteria

$$\left|\frac{\phi_{ij}^{r} - \phi_{ij}^{r-1}}{\phi_{ij}^{r}}\right| \leqslant 10^{-5} \quad (20)$$

and

$$\left|\frac{\overline{Nu}^{r} - \overline{Nu}^{r-1}}{\overline{Nu}^{r}}\right| \leqslant 10^{-4} \quad (21)$$

have been met. In the above expressions, r refers to any particular time level.

RESULTS AND DISCUSSION

The influence of governing physical parameters, such as the Rayleigh number Ra, Prandtl number Pr and various material parameters (Δ, B and λ) on the flow and thermal fields for the buoyancy driven flows in rectangular enclosures are thoroughly explored. The effects of geometric parameters, such as the length, number and location of the discrete heat sources, on the heat transfer characteristics within the enclosure are also examined. Owing to the limitation of pages, the discussion is restricted to a square enclosure, i.e. $A = 1$. The bulk of the results is obtained for cases with $Ra = 10^5$ and Pr[10]. For the sake of comparison, solutions for Newtonian fluid are also investigated and it is shown that significant differences in thermal and flow phenomena are found between them. An accuracy test of the present numerical calculation has made for Newtonian fluid with isothermal case at $Pr = 6.983$, $Ra = 1.4 \times 10^5$, and $A = 1$. The Nusselt number found in this study is $\overline{Nu} = 5.5335$, which is in good agreement with the result ($\overline{Nu} = 5.55$) of Cormack *et al.* [17].

Contours of isotherms and velocity vectors

The isotherms and velocity vectors in the enclosure with a centrally located single isoflux heat source ($Y = 0.5$ and $\varepsilon = 0.2$), two symmetrical equal-powered isoflux heat sources ($Y1 = 0.3$, $Y2 = 0.7$ and $\varepsilon_1 = \varepsilon_2 = 0.2$) and a fully heated vertical wall are shown in Fig. 2 for $Ra = 10^7$. It can be seen that the core region of circulation locates close the upper wall for the case of a centrally located heat source. A much greater temperature gradient in the vicinity of heat source is shown in the figure. Somewhat similar behavior is attained for the case of two symmetrically located heat sources except the isotherms as well as the velocity vectors are evenly distributed. In case of a fully heated vertical wall, it is shown that the isotherms are thoroughly distributed in the whole region of the enclosure and a great core region in the center of enclosure is found as well. The effect of a high-powered isoflux source on the thermal and flow fields is illustrated in Fig. 3 for $Ra = 10^7$. In the plots of isotherms, the isothermal lines are more uniformly distributed in the enclosure if the high-powered heat source is located under the low-powered one. The above-mentioned feature can be used to explain the streamline patterns. The high-powered heat source has denser temperature gradient in the lower half region and, thus, induces convective enhancement. Therefore, the stream function is higher and two secondary circulation cells are seen in the enclosure.

Effect of material parameters

Three material parameters, Δ, B, and λ, which characterize micropolar fluid, are included in the study. The effect of Δ on flow field for a single isoflux heat source ($Y = 0.5$ and $\varepsilon = 0.2$) is shown in Figs. 4 and 5. The maximum value of microrotation $\upsilon_{\max}$ increases as Δ is increased. However, the value of $\Psi_{\max}$ decreases with increasing value of Δ. The relationship between the average Nusselt number $\overline{Nu}$ and material parameter Δ, which is to be pointed in Fig. 9, can be explained appropriately with the aid of this figure. Since an increase in Δ results in a decrease in the strength of flow circulation ($\Psi_{\max}$), thus the rate of heat transfer generally decreases as the parameter Δ increases. Figure 5 shows the contour lines of angular velocity υ on the vertical mid-plane $X = 0.5$ in a square enclosure with Ra and Δ as parameters. The dependence of υ on stream function Ψ is obviously found in the figure, i.e. the value of υ attains its maximum in the core region, decreases gradually away from the core and approaches zero near the boundary $Y = 0$ and 1. The value of υ increases when controlled parameter Δ or Ra increased. Thus, it is concluded from Fig. 5 that the strength of υ depends largely on the field of stream function for constant value of Δ or Ra. The effect of parameter λ on the maximum values of υ and Ψ in a square enclosure with a centrally located

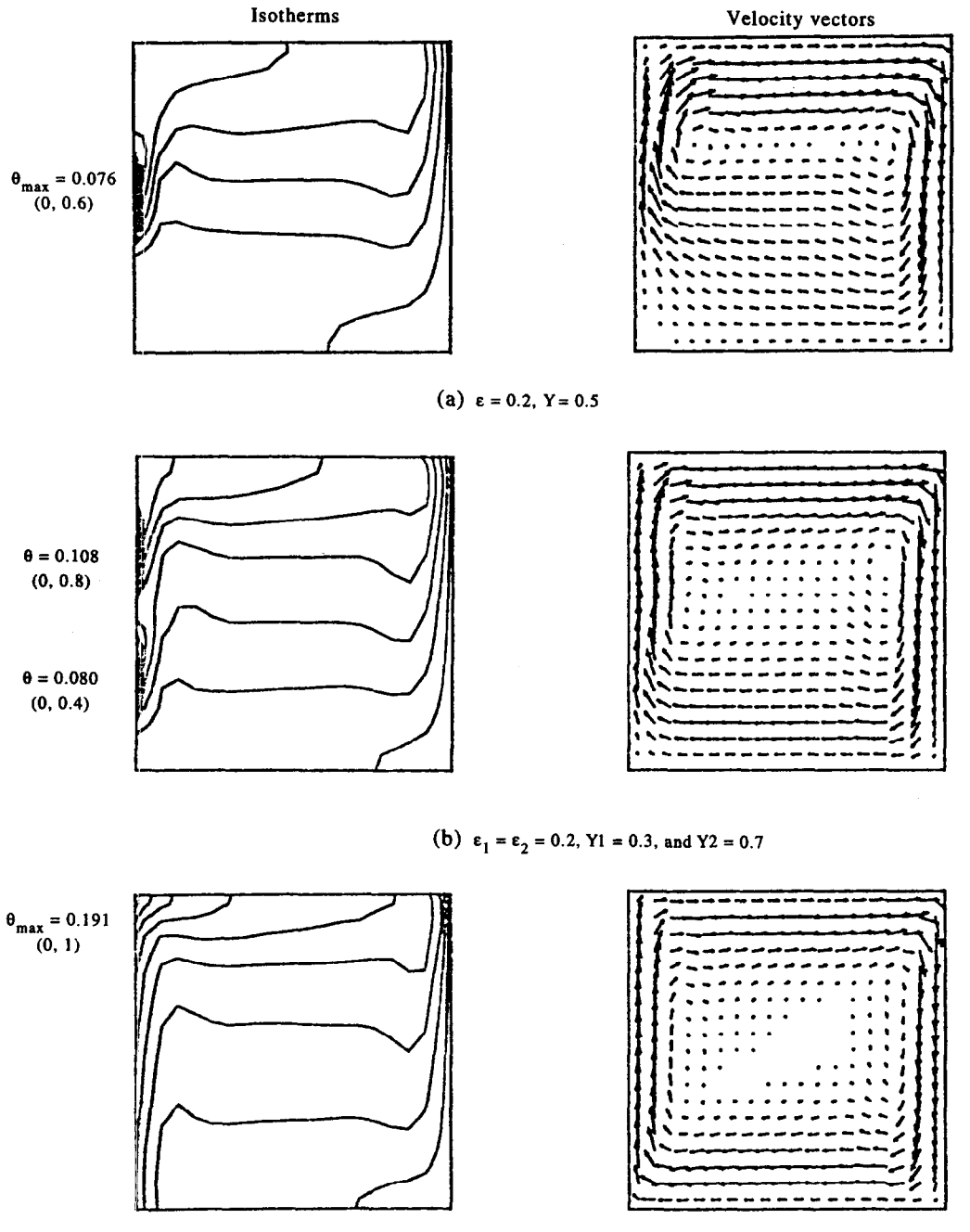

Fig. 2. Isotherms and velocity vectors for different configurations of the isoflux heat source ($B = 0.1$, $\Delta = 2 = 1$, $n = 1$, $Ra = 10^7$).

single heat source is shown in Fig. 6. From the figure shown it is observed that, as λ increases, the value of υ_{max} decreases sharply for $\lambda < 1$, continues gradually for $\lambda > 1$ and then approaches zero for large value of $\lambda(\lambda \to \infty)$. In addition, it also indicates the dependence of Ψ_{max} on parameter λ. As can be seen, variation of Ψ_{max} with λ is very small and can be neglected. The effect of microinertia parameter B on the fluid flow field is shown in Fig. 7. The enclosure studied is restricted to the one with a centrally located single heat source for the reason of comparison. A similar feature of the variation of Ψ_{max} with λ is also found, i.e. the influence of B on the value of Ψ_{max} is negligibly small. However, the increase of υ_{max} is linearly proportional to that of B, as is displayed later in Table 1, although the dependence of Ψ_{max} on both λ and B is negligibly small, the value of $\overline{Nu}$ in the enclosure is decreased with an increase of λ, but is increased with

Table 1. Numerical results for a centrally located heat source ($\varepsilon = 0.2$ and $Y = 0.5$)

B	Δ	λ	n	Ra	Ψ_{max}	v_{max}	θ_{max}	$\overline{Nu}$
0.10	5	1	0	10^4	0.55	0.273	0.345	2.975
—	—	—	—	10^5	4.88	—	0.171	6.551
0.01	5	1	0	10^5	2.46	0.139	0.248	4.350
0.05	5	1	0	10^5	2.46	0.684	0.248	4.353
0.10	5	1	0	10^5	2.48	2.580	0.246	4.386
0.10	0.5	1	0	10^5	4.33	0.221	0.187	5.962
0.10	1	1	0	10^5	3.94	0.401	0.199	5.572
0.10	2	1	0	10^5	3.30	0.736	0.213	5.161
0.10	5	0.5	0	10^5	2.48	2.583	0.246	4.386
0.10	5	2	0	10^5	2.46	0.683	0.247	4.375
0.10	5	5	0	10^5	2.46	0.277	0.248	4.350
0.10	1	1	0	10^6	7.32	0.745	0.121	9.437
0.10	1	1	0	10^7	12.80	1.280	0.076	15.36
0.10	1	1	0.5	10^5	3.95	170.2	0.199	5.576
0.10	1	1	0.5	10^7	13.14	3324	0.071	16.40

— denotes a Newtonian fluid.

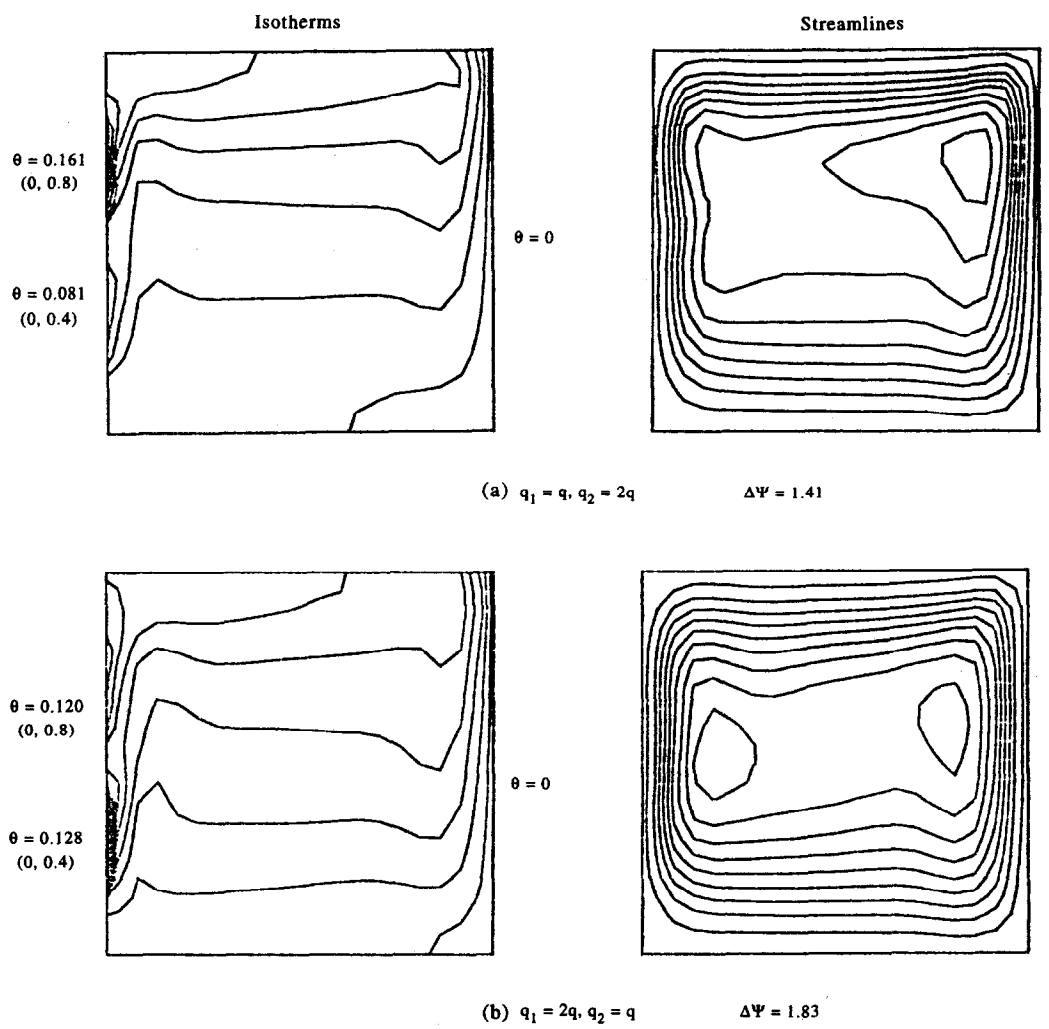

Fig. 3. Isotherms and streamlines for different locations of low- and high-powered isoflux sources ($B = 0.1$, $\Delta = \lambda = 1$, $n = 1$, $\varepsilon_1 = \varepsilon_2 = 0.2$, $Y1 = 0.3$, $Y2 = 0.7$, $Ra = 10^7$).

an increase of B. It is noted that the augmentation of the microrotation term somewhat enlarges the rate of heat transfer in the enclosure.

Effect of microrotation boundary condition

The effect of microrotation boundary condition on the coefficient of heat transfer is indicated in Fig. 8.

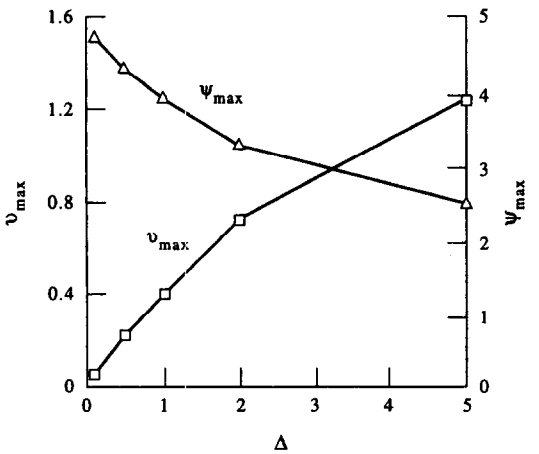

Fig. 4. Effect of vortex viscosity on stream function and microrotation for a centrally located isoflux heat source ($B = 0.1$, $\lambda = 1$. $n = 0$, $\varepsilon = 0.2$, $Y = 0.5$, $Ra = 10^5$).

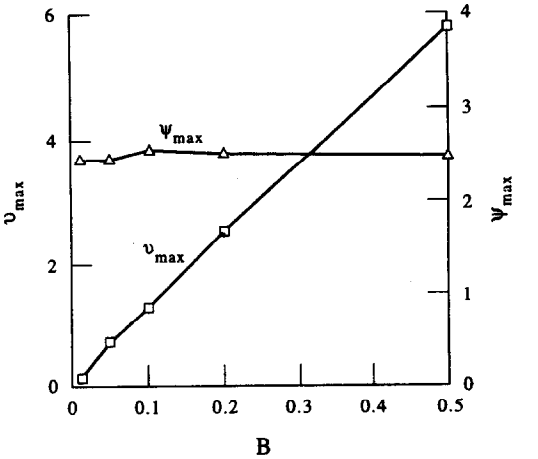

Fig. 7. Effect of microinertia on stream function and microrotation for a centrally located isoflux heat source ($\Delta = 5$, $\lambda = 1$, $n = 0$, $\varepsilon = 0.2$, $Y = 0.5$, $Ra = 10^5$).

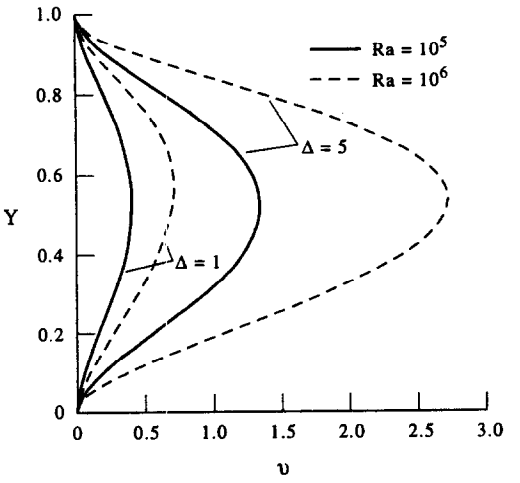

Fig. 5. Mid-sectional microrotation distributions for a centrally located isoflux heat source ($B = 0.1$, $\lambda = 1$, $n = 0$, $\varepsilon = 0.2$, $Y = 0.5$).

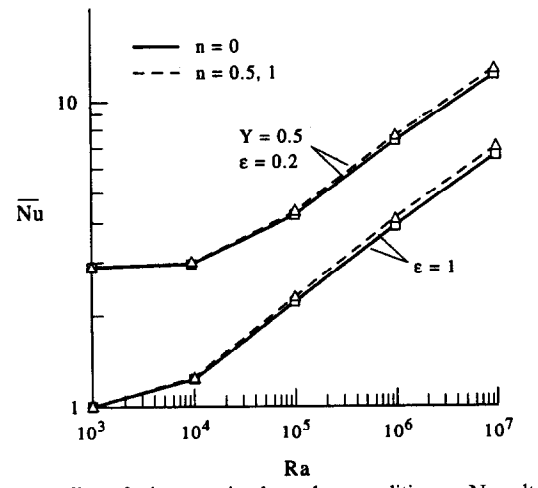

Fig. 8. Effect of microrotation boundary condition on Nusselt number for isoflux heat source ($B = 0.1$, $\Delta = 5$, $\lambda = 1$).

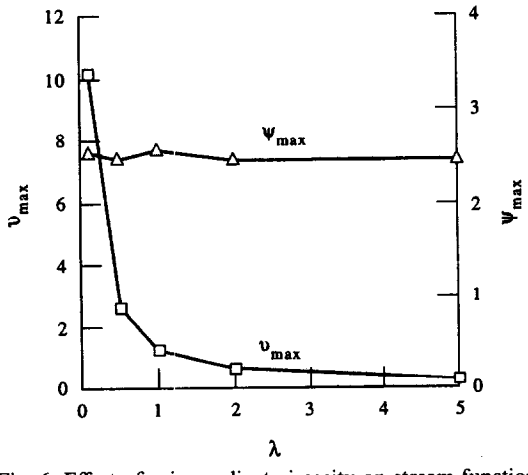

Fig. 6. Effect of spin gradient viscosity on stream function and microrotation for a centrally located isoflux heat source ($B = 0.1$, $\Delta = 5$, $n = 0$, $\varepsilon = 0.2$, $Y = 0.5$, $Ra = 10^5$).

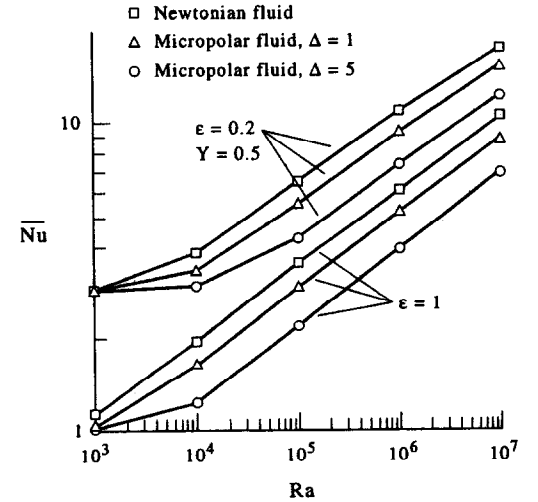

Fig. 9. Variation of Nusselt number with *Ra* for isoflux case ($B = 0.1$, $\lambda = 1$, $n = 0$).

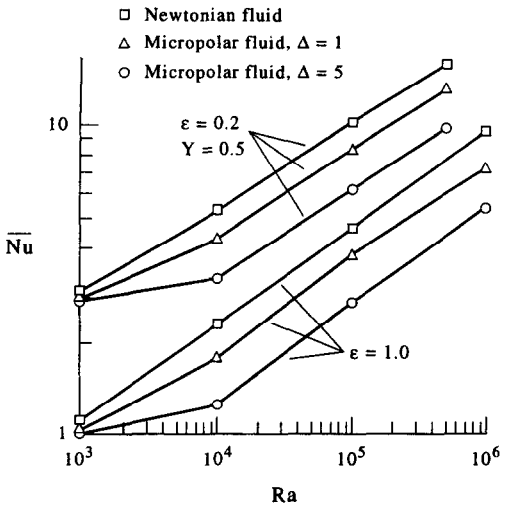

Fig. 10. Variation of Nusselt number with *Ra* for isothermal case ($B = 0.1$, $\lambda = 1$, $n = 0$).

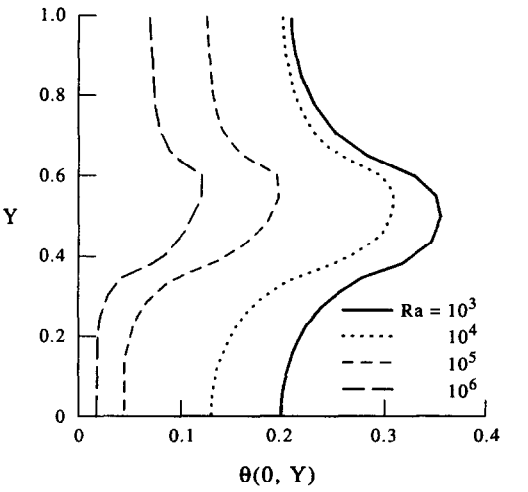

Fig. 11. Temperature distributions along heated wall for a centrally located heat source ($B = 0.1$, $\Delta = \lambda = 1$, $n = 1$, $\varepsilon = 0.2$, $Y = 0.5$, isoflux case).

As n increases, the value of $\overline{Nu}$ increases. It is because particles are not free to rotate near the surface for $n = 0$, whereas the microrotation term is augmented and induces flow enhancement as n increases to 0.5. Line for $n = 1$ does not differ greatly from that for $n = 0.5$ and they are plotted together in the figure.

Effect of Rayleigh number

Figures 9 and 10 show the relationship between $\overline{Nu}$ and *Ra* for both cases, i.e. isoflux heat source and isothermal heat source, respectively. As expected, it is found that values of $\overline{Nu}$ increase with increasing *Ra* and the curves are directly linear in the log $\overline{Nu}$ vs log *Ra* plots for *Ra* greater than a certain value, which is significantly different for various fluids. It is noted that for the case of a centrally located discrete heat source with $\varepsilon = 0.2$, the values of $\overline{Nu}$ for a micropolar fluid are seen to be lower as compared to a Newtonian fluid. Because a micropolar fluid has larger value of flow viscosity than a Newtonian fluid due to the enhancement of vortex viscosity that is in company with a micropolar fluid. Thus, the strength of natural convection flow that occurs in the enclosure is accordingly diminished and less heat is transferred from the discrete heat source. It is also found in the same figure that the values of $\overline{Nu}$ get lower for a micropolar fluid with larger vortex viscosity parameter Δ. Figure 10 shows that the case of isothermal discrete heat source follows the same trend as isoflux heat source. Figure 11 shows the variation of the temperature distribution of the wall on which the discrete heat source is centrally located for $\Delta = \lambda = 1$ and various values of *Ra*. It is found that the surface temperature on the discrete heat source is certainly lower for higher values of *Ra* (which is obvious from equation (6)). As a consequence of the lower surface temperature of heat source, the heated wall, i.e. the source embedded wall, has a lower wall temperature due to the convection effect. This is because conduction is responsible for

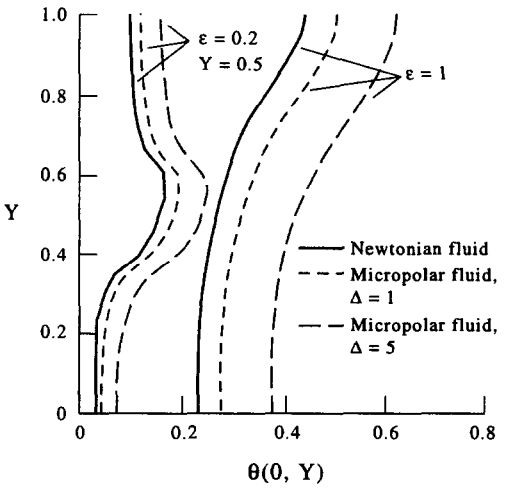

Fig. 12. Temperature distributions along heated wall for centrally located source and fully heated wall ($B = 0.1$, $\lambda = 1$, $n = 0$, $Ra = 10^5$, isoflux case).

the major part of heat transfer quantity in the system. At lower value of *Ra*, the surface temperature distribution on the heated wall is found to be vertically symmetric for $Ra = 10^3$.

Comparison between fluid characteristics

As shown in Figs. 9 and 10, a micropolar fluid with large vortex viscosity has low Nusselt number, i.e. less heat transfer occurred in the enclosure. This phenomenon reflects the fact that increasing the value of vortex viscosity results in an enhancement of the total viscosity in fluid flow and, thus, the heat transfer is retarded. The effect of vortex viscosity on the surface temperature is clearly displayed in Fig. 12. The wall temperatures are higher for micropolar fluid with larger vortex viscosity. In addition, a Newtonian fluid has lower surface temperature distribution in comparison with micropolar fluid. The effect of spin gradi-

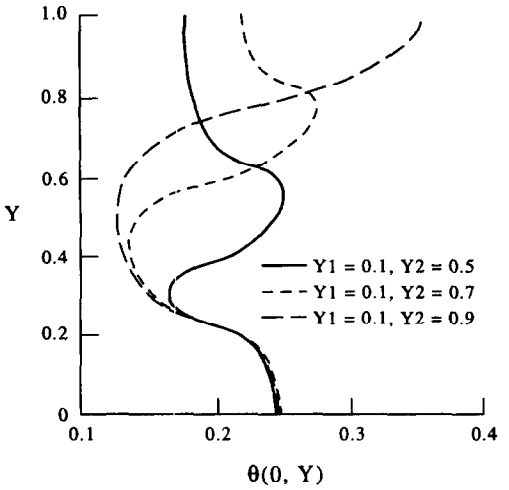

Fig. 13. Effect of heater q_2 on temperature distributions along heated wall ($B = 0.1$, $\Delta = \lambda = 1$, $n = 0$, $\varepsilon_1 = \varepsilon_2 = 0.2$, $Ra = 10^5$, isoflux case).

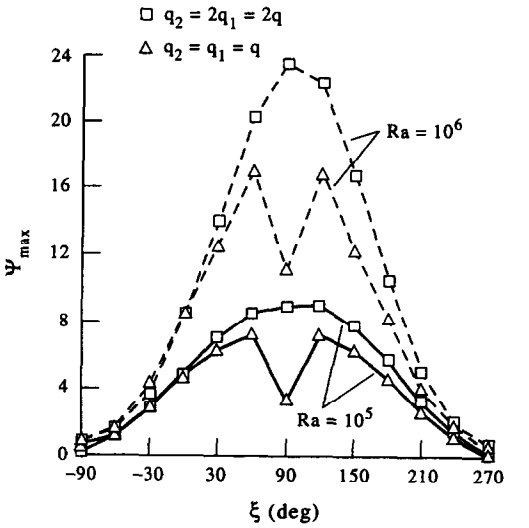

Fig. 14. Variation of stream function with tilting angle ($B = 0.1$, $\Delta = \lambda = 1$, $n = 0$, $\varepsilon_1 = \varepsilon_2 = 0.2$, $Y1 = 0.3$, $Y2 = 0.7$, isoflux case).

ent viscosity parameter λ on heat transfer is shown in Table 1. Since the spin gradient viscosity term consumes a portion of energy in the system to develop the fluid motion, hence an increase in λ causes a decrease of Nusselt number $\overline{Nu}$.

Effect of heat source location

The case of many heat sources mounted on a vertical insulated wall is simulated by the same model as before. Figure 13 shows the surface temperature variations for a two-components arrangement with $\varepsilon_1 = \varepsilon_2 = 0.2$, $q_1 = q_2 = q$, $Y1 = 0.1$ and $Y2 = 0.5$–0.9. The surface temperature distributions along the heated wall are significantly different for the three cases. As the location of the upper heat source shifts from $Y2 = 0.5$ to 0.9, the maximum surface temperature increases from the mid-height to the top along the heated wall. Furthermore, the location of the upper heat source has negligible effect on the lower one's temperature. It is because the fluid moves upward along the heated wall by natural convection, and, thus, heat transfer downward occurs by diffusion. Figures 14–16 demonstrate the effect of nonequal-powered heat sources on the maximum value of stream function Ψ_{max}, the maximum value of surface temperature θ_{max} and temperature distribution on hot wall. In these figures, the locations of the heat sources are illustrated by the tilting angle ξ. It is noted that the positions of the heat sources, with heat transfer flux q_1 and q_2, respectively, do happen to be reversed on the vertical wall for $\xi = 0$ and 180°. As expected, the plots of Ψ_{max} and θ_{max} display symmetry about $\xi = 90°$ for the case of equal-powered heat source, i.e. $q_1 = q_2 = q$. A steep jump is found in the variation of Ψ_{max} against tilting angle ξ at $\xi = 90°$ in that case as well. As the heated wall is placed horizontal, i.e. $\xi = 90°$, two main circulation cells are achieved (which are not shown in this paper) in the enclosure, the values of stream function are smaller and, thus,

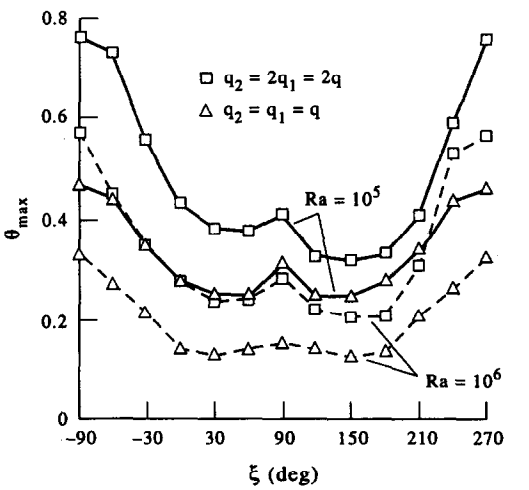

Fig. 15. Variation of maximum temperature on heated wall with tilting angle ($B = 0.1$, $\Delta = \lambda = 1$, $n = 0$, $\varepsilon_1 = \varepsilon_2 = 0.2$, $Y1 = 0.3$, $Y2 = 0.7$, isoflux case).

the strength of natural convection field decreases. However, only one main circulation cell is found for the case of nonequal-powered heat sources. This is due to the fact that the difference of heat flux between the two heat sources promotes the buoyancy induced flow. Hence, the maximum stream function Ψ_{max} retains continuous variation when it is plotted against the tilting angle ξ, as shown in Fig. 14. In the case of nonequal power heat sources, i.e. $2q_1 = q_2 = 2q$, the distribution lines of Ψ_{max} and θ_{max} vs ξ are skew symmetric about $\xi = 90°$. It illustrates the significant effect of the heated component arrangement. In Fig. 14, the values of Ψ_{max} at $\xi = 0$ and 180° are 4.93 and 5.78, respectively. It indicates the fact that putting the high-powered heat source under the low-powered one on the vertical heated wall gives rise to a larger stream function, which denotes a strong flow circulation and

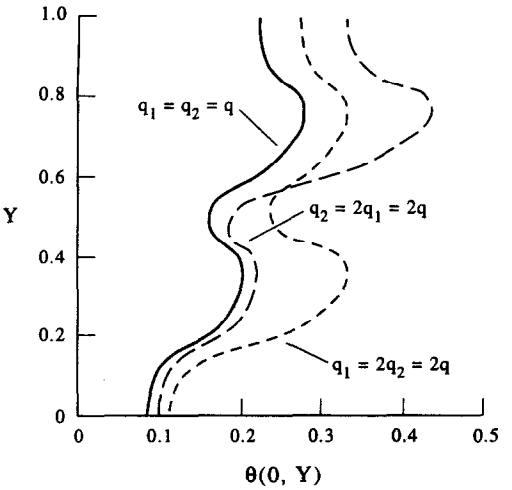

Fig. 16. Temperature distributions along heated wall ($B = 0.1$, $\Delta = \lambda = 1$, $n = 0$, $\varepsilon_1 = \varepsilon_2 = 0.2$, $Y1 = 0.3$, $Y2 = 0.7$, $Ra = 10^5$, isoflux case).

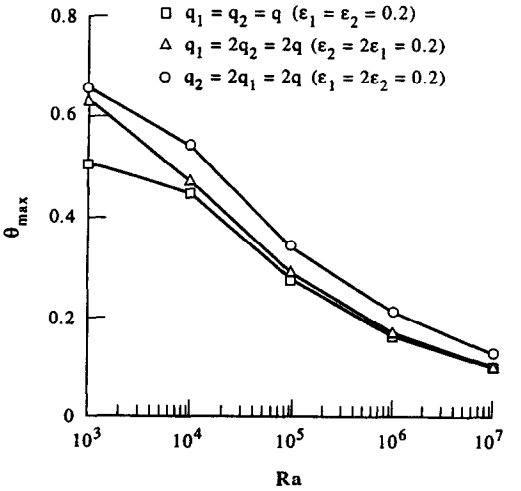

Fig. 17. Effect of heater intensity on temperature of heated wall ($B = 0.1$, $\Delta = \lambda = 1$, $n = 0$, $Y1 = 0.3$, $Y2 = 0.7$, isoflux case).

is helpful in obtaining a lower heat source surface temperature (Fig. 15). It is also shown in Fig. 14 that the values of Ψ_{max} for the two different arrangements of heat sources are very close for $-90° \leqq \xi \leqq 0°$. In contrast, the differences in values of Ψ_{max} between the two cases as mentioned are considerably larger for $30° \leqq \xi \leqq 180°$. Furthermore, the enclosure always retains its lower surface temperature if the high-powered heat source is placed below the low-powered one, as shown in Fig. 15. Figure 16 displays further the surface temperature along the vertical heated wall for the three different cases as indicated. For the equal-powered heat sources condition, the upper portion of the heated wall has lower temperature due to the enhancement of natural convection. The upper heat source attains very high surface temperature if the high-powered heat source is located over another one. The temperature variations along the wall show that the top high-powered heat source has a negligible effect on bottom source's temperature. However, in comparison to the previous condition, the lower high-powered heat source has a much higher temperature as well as a significant effect on top source's temperature. The same result has been pointed out by Afrid and Zebib [5] for a vertical wall in the open region. Thus, it is recommended to install the high-powered heat source at the bottom position if the temperature limitation is a main design consideration.

Effect of heater size and intensity

Figure 17 illustrates the dependence on heater size and heat flux in a square enclosure with two symmetrically located heat sources on the vertical wall. The heat transfer rate for the three cases, with variable power intensity (e.g. $q_1 = q$ or $2q$) and heat source size (e.g. $\varepsilon_1 = 0.1$ or 0.2), is the same theoretically. It is shown that the selection of high-powered intensity, but short, source length for the top heat source results in a higher temperature, whereas significant low values of θ_{max} can be seen if the two heat sources are interchanged in the previous condition.

Some numerical results are tabulated in Table 1. It is shown that the values of stream function and $\overline{Nu}$ of micropolar fluids are generally smaller as compared to a Newtonian fluid. Both values of υ_{max} and Ψ_{max} are significantly affected by vortex viscosity Δ. However, parameters B and λ have considerable effect on micro-rotation field, but negligible influence on stream function and heat transfer coefficient $\overline{Nu}$. The numerical predictions of the flow feature displayed by the micropolar fluids and a quantitative comparison with the traditional Newtonian fluid are of main interest in this investigation. Thus, only computational results are available.

CONCLUSION

Natural convection of micropolar fluids in an enclosure with isolated heat sources, either isothermal or isoflux, has been analyzed numerically. The computation of the temperature and velocity fields in the enclosure are also performed for a Newtonian fluid for comparison reason. In both fluids, conduction is observed to be the predominant mechanics for heat transfer for $Ra < 10^3$, even small circulation occurs for all $Ra > 0$.

The numerical results indicate that the average Nusselt number is lower for a micropolar fluid, as compared to a Newtonian fluid. It is shown that high-powered heat source has negligible effect on the lower one's temperature, whereas it has significant effect on the higher one's temperature.

The numerical study performed shows a very significant effect of microstructure on the convective heat transfer. The value of maximum microrotation term υ_{max} increases when either vortex viscosity or micro-inertia increases. Conversely, the value of υ_{max} decreases as the spin gradient viscosity increases. Con-

siderable effects on both thermal and velocity fields are found for variation of vortex viscosity.

It is observed that the heat transfer rate is quite sensitive to the microrotation boundary conditions. The heat transfer rate increases due to the enhancement of flow velocities for weak concentration flow ($n = 0.5$ or 1).

Acknowledgements—This work was supported by the National Science Council in Taiwan under Grant no. NSC 83-0117-C-151-014 E.

REFERENCES

1. Ostrach, S., Natural convection in enclosures. *Advances in Heat Transfer*, 1972, **8,** 161–227.
2. Catton, I., Natural convection in enclosures. *Proceedings of The 6th International Heat Transfer Conference*, Toronto, Canada, 1978, pp. 13–21.
3. Chu, H. H., Churchill, S. W. and Patterson, C. V. S., The effect of heat size, location, aspect ratio and boundary conditions on two dimensional, laminar, natural convection in rectangular channels. *ASME Journal of Heat Transfer*, 1976, **96**(2), 194–201.
4. Turner, B. L. and Flack, R. D., The experimental measurement of natural convection heat transfer in rectangular encloses with concentrated energy sources. *ASME Journal of Heat Transfer*, 1980, **102**(2), 236–241.
5. Afrid, M. and Zebib, A., Natural convection air cooling of heated components mounted on a vertical wall. *Numerical Heat Transfer*, Part A, 1989, **15,** 243–259.
6. Keyhani, M., Prasad, V. and Cox, R., An experimental study of natural convection in a vertical cavity with discrete heat sources. *ASME Journal of Heat Transfer*, 1988, **110**(3), 616–624.
7. Refai, G. and Yovanovich, M. M., Numerical study of natural convection from discrete heat sources in a vertical square enclosure. *AIAA Journal of Thermophysics*, 1992, **6**(1), 121–127.
8. Eringen, A. C., Simple microfluids. *International Journal of Engineering Science*, 1964, **2,** 205–217.
9. Eringen, A. C., Theory of micropolar fluids. *Journal of Mathematical Mechanics*, 1966, **16**(1), 1–16.
10. Eringen, A. C., Theory of thermomicrofluids. *Journal of Mathematical Analysis Applications*, 1972, **9,** 480–496.
11. Jean, S. K. and Bhattacharyya, S. P., The effect of microstructure on the thermal convection in a rectangular box of fluid heated from below. *International Journal of Engineering Science*, 1986, **24,** 69–76.
12. Chen, C. K. and Hsu, T. H., Natural convection of micropolar fluids in an enclosure. *ASME/JSME Thermal Engineering Process*, 1991, **1,** 199–205.
13. Jena, S. K. and Mathur, M. N., Similarity solutions for laminar free convection flow of a thermomicropolar fluid past a nonisothermal vertical flat plate. *International Journal of Engineering Science*, 1981, **19,** 1431–1439.
14. Ahmadi, G., Self-similar solutions of incompressible micropolar boundary layer flow over a semi-infinite plate. *International Journal of Engineering Science*, 1976, **14,** 639–646.
15. Peddieson, J., An application of the micropolar fluid model to the calculation of a turbulent shear flow. *International Journal of Engineering Science*, 1972, **10,** 23–32.
16. Rubin, S. G. and Graves, R. A., Viscous flow solution with a cubic spline approximation. *Computers and Fluids*, 1975, **1,** 1–36.
17. Cormack, D. E., Leal, L. G. and Seinfeld, J. H., Natural convection in a shallow cavity with differentially heated end walls, Part 2: numerical solutions. *Journal of Fluid Mechanics*, 1074, **65,** 231–246.